Journal of Sound and Vibration (2001) **242**(3), 445–473
doi:10.1006/jsvi.2000.3374, available online at http://www.idealibrary.com on IDEAL®

AN INVESTIGATION OF POWER FLOW IN THE MID-FREQUENCY RANGE FOR SYSTEMS OF CO-LINEAR BEAMS BASED ON A HYBRID FINITE ELEMENT FORMULATION

N. VLAHOPOULOS AND X. ZHAO

Department of Naval Architecture and Marine Engineering, The University of Michigan, 2600 Draper Road, Ann Arbor, MI 48109-2145, *U.S.A.*

(*Received* 6 *January* 2000, *and in final form* 25 *August* 2000)

A hybrid finite element analysis (hybrid FEA) is employed for investigating power flow characteristics for systems of co-linear beams in the mid-frequency range. The importance of capturing power re-injection and power re-radiation effects in the solution is demonstrated. The dependency of the power flow characteristics of a system in the mid-frequency range on the rigidity, mass, and damping properties of its components is determined. Both the hybrid FEA and analytical solutions are employed for analyses in order to establish the viability of the hybrid FEA as a simulation technology in the mid-frequency range. Results from a high-frequency method are compared to hybrid FEA solutions in order to demonstrate the importance of capturing the resonant effects in mid-frequency computations.

1. INTRODUCTION

The frequency spectrum where simulation methods can be utilized for vibration analysis can be divided into three regions: low-, mid-, and high frequency. The low-frequency region is defined as the frequency range where all components contain a small number of wavelengths (short members). Due to the relative large size of the wavelengths with respect to the size of each component, small uncertainties in the properties of the short members will not impact their distinctly resonant behavior. By taking into account the definition of the modal overlap as the resonance bandwidth divided by the average frequency spacing between resonance frequencies it is expected that short members will have low modal overlap values due to their resonant behavior. The short members are expected to be lightly damped, since high damping will increase the resonance bandwidth, reduce the resonance characteristics, and increase the modal overlap. Conventional finite element analysis (FEA) is a practical numerical approach for simulating low-frequency vibrations [1–3].

The high-frequency region is defined as the frequency range where all component members of a system are long with respect to a wavelength (long members). Due to the relative small size of the wavelengths with respect to the size of each component small uncertainties in the properties of the long members lead to behavior that can be represented as incoherent. Long members are expected to exhibit considerably higher modal overlap than the short members, since resonant effect are not present. Statistical energy analysis (SEA) [4–8], and energy finite element analysis (EFEA) [9–16] can be used for vibro-acoustic simulations at high frequencies. Both SEA and EFEA provide

0022-460X/01/180445 + 29 $35.00/0

meaningful results for the ensemble average response of each member and of the system. The two methods represent a modal (SEA) and a wave approach (EFEA) for addressing high-frequency analysis. Extensive discussion of the similarities between the two methods and correlation results for complex marine structures have been presented [16].

The mid-frequency region is defined as the frequency range where some members in a system are long while other members are short. In the mid-frequency range the FEA method requires a prohibiting large number of elements to perform an analysis due to the presence of the long members. In addition, high computational resources are required in order to produce frequency-averaged FEA results that constitute a meaningful representation of the ensemble-average response of a system with uncertainty. The energy methods (SEA and EFEA) contain assumptions that are valid when all components of a system are long. Based on the assumption of high modal overlap, the SEA formulation considers the normal modes within a frequency band as equally probable, containing the same amount of energy, and demonstrating an equal amount of damping [4]. The assumption of a small wavelength with respect to the dimension of a member in the EFEA is similar to the assumption of high modal overlap in SEA. The requirement for small wavelength in the EFEA allows to neglect the near-field effects in the wave solution and allows to consider a reverberant behavior for all the members in a system during the development of the governing differential equations [10–12]. Thus, the energy methods cannot capture the resonant effects in the behavior of a system in the mid-frequencies. The resonant effects are generated from the presence of the short members.

In the energy methods the amount of power transferred between members at a joint is estimated in terms of coupling loss factors (in SEA) or power transfer coefficients (in EFEA). The value of the coupling loss factors or the power transfer coefficients are computed from analytical solutions of semi-infinite members [17]. The computations are meaningful when the connected members are long, thus the power transfer characteristics of the long members can be considered the same with the power transfer characteristics of the semi-infinite members. The requirement for high modal overlap is necessary because the information produced by the analytical solutions of the semi-infinite members captures the exchange of power flow between members when there is an equal amount of coupling between the normal modes of the members. If large differences exist in the power flow due to the distinct resonant behavior of the short members, then the power transfer characteristics cannot be estimated properly from analytical solutions of semi-infinite members.

The basic theoretical formulation of the hybrid FEA employed in this paper for mid-frequency computations has been presented previously [18]. The hybrid FEA is based on coupling conventional FEA models of short members to EFEA models of long members. The joints between long and short members are modelled by combining analytical solutions of semi-infinite members that represent the long members to FEA numerical models for the short members. Two sets of data are produced from the coupling process. The first set is comprised of power transfer coefficients for each EFEA member at a joint with a short member. The computed power transfer coefficients contain information for the resonant behavior of the short members and the damping that can be present in the short members. The second set of data is comprised of relationships between the primary variables of the EFEA model and the primary variables of the FEA model at a joint between long and short members. A major advantage offered from the wave-based formulation of the EFEA is the distinction between the energy (and the power) associated with waves travelling towards and away from a joint. At a joint between a long and a short member only the energy associated with the impinging wave contributes to the excitation of the short member. Thus, when multiple members are connected together, effects of strong coupling, power

re-injection [19, 21], indirect power flow [20], and power re-radiation [19, 21] can be captured correctly by the hybrid finite element solution.

The scope of this paper is to utilize the simulation capabilities of the hybrid FEA in order to investigate power flow characteristics for a system of three co-linear beams in the mid-frequency range. The system is comprised of two long beams connected by a short one. The effect of the combined stiffness and damping characteristics of the coupled short member on the power flow is identified. Power flow concepts that have been demonstrated in the past by systems of oscillators or by analytical solutions of two continuous subsystems [19–23] are also investigated by the hybrid FEA. Specifically, the following power flow concepts are presented

(1) Power re-injection [19, 21] and power re-radiation [19, 21] effects are present in the hybrid FEA solution.
(2) The amount of power transferred between long members is strongly affected by the coupling damping and coupling rigidity exhibited by the short member.
(3) The power flow between long members can be controlled by properly selecting the flexural and damping characteristics of the short member.
(4) The power transferred between the two long members depends on the relative bending rigidity exhibited by the two long members and the coupling damping ratio between short and long members.

The theoretical background of the hybrid FEA is reviewed first. The specific power flow variables that are required as output by the analyses presented in this paper are derived from the primary variables of the FEA formulation of the short members. Results from hybrid FEA simulations and from analytical solutions are presented for all the analyzed systems in order to investigate the outlined power flow concepts and further validate the hybrid FEA method. EFEA results are also compared to hybrid FEA solutions in order to demonstrate the deficiency of a high-frequency method in performing mid-frequency computations when resonant effects are important.

2. BACKGROUND ON THE HYBRID FINITE ELEMENT ANALYSIS

The primary concept of the hybrid finite element formulation is to utilize low-frequency FEA models for deriving energy information for the short members, and to integrate them with EFEA models representing the long members. Due to the presence of the long members in the system, the response of the all members will remain incoherent inasmuch as the short members will be subjected to an incoherent excitation at the points where they are connected to the long members. Previous work has demonstrated how low-frequency vibro-acoustic models can be analyzed when they are subjected to incoherent excitation [24]. The EFEA is selected to be coupled with the low-frequency method because it constitutes a wave approach for high-frequency solutions and it is based on a spatial discretization of the system that is being modelled. Thus, it is possible to develop appropriate interface conditions at the joints between the primary variables of the EFEA formulation and the primary variables of the FEA formulation since both can be associated with displacement properties at the joints.

In EFEA the energy density is space-averaged over a wavelength and time-averaged over a period. The space- and time-averaged energy density constitutes the primary variable of the formulation [9–15]. The governing differential equation associated with one of the

bending degrees of freedom in a beam is

$$\frac{-c_g^2}{\eta\omega}\frac{\mathrm{d}^2\langle \underline{e}\rangle}{\mathrm{d}x^2} + \eta\omega\langle \underline{e}\rangle = \langle \underline{Q}_{in}\rangle, \tag{1}$$

where c_g is the group speed of the bending waves, η the hysterisis damping factor, ω the radial frequency, $\langle \underline{Q}_{\mathrm{in}}\rangle$ the external input power, and $\langle \underline{e}\rangle$ the time- and space-averaged energy density. A finite element approach is employed for solving equation (1) numerically, resulting in [25]

$$\lfloor E^e \rfloor_i \{e^e\}_i = \{F^e\}_i + \{Q^e\}_i, \tag{2}$$

where superscript "e" indicates element-based quantities, subscript "i" indicates the ith element, $\{e^e\}_i$ = vector is nodal values for the time- and space-averaged energy density for the ith element, $\lfloor E^e \rfloor_i$ is the system matrix for the ith element, $\{F^e\}_i$ the vector of external input power at the nodal locations of the ith element, and $\{Q^e\}_i$ the vector of internal power flow at the boundary locations of the ith element. In EFEA the term $\{Q^e\}_i$ provides the mechanism for connecting elements together across discontinuities [25]. In the hybrid FEA formulation, $\{Q^e\}_i$ provides the mechanisms for prescribing the power flow between long and short members.

In EFEA at positions where different members are connected the energy density is discontinuous. The corresponding boundary between the elements defines a joint location. Therefore, during the assembly of the global system the element matrices do not couple, and the values of the internal power flow at the common node do not overlap to cancel each other. Instead, they remain as variables on the right-hand side of the equation

$$\begin{bmatrix} [E^e]_i & \\ & [E^e]_j \end{bmatrix} \begin{Bmatrix} \{e^e\}_i \\ \{e^e\}_j \end{Bmatrix} = \begin{Bmatrix} \{F^e\}_i \\ \{F^e\}_j \end{Bmatrix} + \begin{Bmatrix} \{Q^e\}_i \\ \{Q^e\}_j \end{Bmatrix}. \tag{3}$$

A special procedure is used for assembling the element matrix into the global matrix equations [25]. A specialized joint element equation is developed to formulate the connection between the discontinuous primary variables at the joint. The values of the power flow at the inter-element nodes corresponding to the two adjacent elements are expressed in terms of the corresponding energy densities [25]:

$$\begin{Bmatrix} Q^e_{ic} \\ Q^e_{jc} \end{Bmatrix} = [J]^i_j \begin{Bmatrix} e^e_{ic} \\ e^e_{jc} \end{Bmatrix}, \tag{4}$$

where subscript "c" indicates the common node between elements "i" and "j", and $[J]^i_j$ is the joint matrix expressing the mechanism of power transfer between elements "i" and "j". The coefficients of the joint matrix are computed by utilizing power transfer coefficients derived from analytical solution of semi-infinite members fully connected to each other, and by taking into account the continuity of the power flow across the joint. Introducing equation (4) into equation (3) results in

$$\left(\begin{bmatrix} [E^e]_i & \\ & [E^e]_j \end{bmatrix} + [JC]^i_j \right) \begin{Bmatrix} \{e^e\}_i \\ \{e^e\}_j \end{Bmatrix} = \begin{Bmatrix} \{F^e\}_i \\ \{F^e\}_j \end{Bmatrix}, \tag{5}$$

where $[JC]^i_j$ is the joint matrix comprising the coefficients of $[J]^i_j$ positioned in the appropriate locations.

In the mid-frequency range, a system is comprised of both long and short members. A hybrid FEA formulation has been presented for mid-frequency computations when the

external excitation is applied on long members of the system [18]. The FEA model of a short member is coupled with analytical solutions of semi-infinite members in order to formulate a hybrid joint. Power transfer coefficients and relationships between EFEA and FEA primary variables are computed by the hybrid joint formulation. By considering a wave incident to the joint from the left semi-infinite member, the continuity conditions for the displacement and the slope, and the equilibrium of force and moment at the joints, a system of equations between the primary variables of the FEA formulation at the joint and the coefficients of the semi-infinite members associated with the reflected and transmitted waves is developed [18]:

$$\begin{bmatrix} 1 & 0 & 0 & 0 & -1 & -1 & 0 & 0 \\ 0 & -1 & 0 & 0 & \mathrm{i}k_m & k_m & 0 & 0 \\ 0 & 0 & 1 & 0 & 0 & 0 & -1 & -1 \\ 0 & 0 & 0 & 1 & 0 & 0 & ik_n & k_n \\ S^m_{11} & S^m_{12} & S^m_{13} & S^m_{14} & \mathrm{i}(EI)_m k_m^3 & -(EI)_m k_m^3 & 0 & 0 \\ S^m_{21} & S^m_{22} & S^m_{23} & S^m_{24} & -(EI)_m k_m^2 & (EI)_m k_m^2 & 0 & 0 \\ S^m_{31} & S^m_{32} & S^m_{33} & S^m_{34} & 0 & 0 & \mathrm{i}(EI)_n k_n^3 & -(EI)_n k_n^3 \\ S^m_{41} & S^m_{42} & S^m_{43} & S^m_{44} & 0 & 0 & (EI)_n k_n^2 & -(EI)_n k_n^2 \end{bmatrix} \begin{Bmatrix} u^m_m \\ \mathrm{d}u^m_m/\mathrm{d}x \\ u^m_n \\ \mathrm{d}u^m_n/\mathrm{d}x \\ C^m_m \\ D^m_m \\ A^m_n \\ B^m_n \end{Bmatrix} = \begin{Bmatrix} 1 \\ \mathrm{i}k_m \\ 0 \\ 0 \\ \mathrm{i}(EI)_m k_m^3 \\ (EI)_m k_m^2 \\ 0 \\ 0 \end{Bmatrix} A^m_m, \tag{6}$$

where superscript "m" is associated with the incident wave from the left member; subscripts "m" and "n" indicate the left and right semi-infinite members respectively, A is the amplitude of the far field right-travelling wave, B the amplitude of the near field right-travelling wave, C the amplitude of the farfield left-travelling wave, D the amplitude of the near field left-travelling wave, k the wave number, EI the bending rigidity, S_{ij} the entries of the FEA matrix of the short member condensed to the four interface degrees of freedom with the long members, u_m, u_n the displacements at the left and right ends of the short beam, respectively, $\mathrm{d}u_m/\mathrm{d}x$, $\mathrm{d}u_n/\mathrm{d}x$ are the slopes at the left and right ends of the short beam respectively. Equation (6) is utilized to derive power transfer coefficients for long members that are connected through a short member and for relationships between the primary variables of the EFEA and FEA formulations at the joints between long and short members. An equation similar to equation (6) can be developed when considering an incident wave from the right semi-infinite member.

By solving the system of equation (6), each one of the eight unknowns can be expressed in terms of the coefficient A^m_m, which is associated with the impinging wave:

$$u^m_m = a^m_1 A^m_m, \quad \mathrm{d}u^m_m/\mathrm{d}x = a^m_2 A^m_m, \quad u^m_n = a^m_3 A^m_m, \quad \mathrm{d}u^m_n/\mathrm{d}x = a^m_4 A^m_m,$$

$$C^m_m = a^m_5 A^m_m, \quad D^m_m = a^m_6 A^m_m, \quad A^m_n = a^m_7 A^m_m, \quad B^m_n = a^m_8 A^m_m. \tag{7}$$

The power transmission coefficient τ_{mn} is the ratio of the transmitted power over the incident power. The power reflection coefficient r_{mm} is the ratio of the reflected power over the incident power. Without loss of generality the coefficient of the impinging wave A^m_m can be considered as a real and positive number. Hence, the power transfer coefficient τ_{mn} for the

right member "n" due to the incident wave in the left member "m" is

$$\tau_{mn} = \frac{q^m_{tran}}{q^m_{inc}} = \frac{(EI)_n k_n^3 \omega |A_n^m|^2}{(EI)_m k_m^3 \omega |A_m^m|^2} = \frac{(EI)_n k_n^3 |A_n^m|^2}{(EI)_m k_m^3 |A_m^m|^2} = \frac{(EI)_n k_n^3}{(EI)_m k_m^3} |a_7^m|^2. \tag{8}$$

The reflection coefficient r_{mm} in the left member "m" due to the incident wave in the same member is

$$\tau_{mn} = \frac{q^m_{refl}}{q^m_{inc}} = \frac{(EI)_m k_m^3 \omega |C_m^m|^2}{(EI)_m k_m^3 \omega |A_m^m|^2} = \frac{|C_m^m|^2}{|A_m^m|^2} = |a_5^m|^2. \tag{9}$$

The derivation of the EFEA power transfer coefficients accounts for the resonant and damping characteristics of the short member. The constants a_5^m and a_7^m that are directly associated with r_{mm} and τ_{mn}, respectively, are computed from the solution to equation (6) which includes all the characteristics of the FEA matrix of the short member condensed to the interface degrees of freedom at the joint. By considering an incident wave originating from the right semi-infinite member, equation similar to equations (8) and (9) can be derived for the power transfer coefficients τ_{nm} and r_{nn}.

When two long members are connected by a short member, the energy density at the edge of the left member at the joint depends on the right travelling wave and its reflection, but at the same time it depends on the amount of power transmitted from the other long member. Thus, the energy density e_m at the connection of the left long member to the short member can be written as

$$\begin{aligned} e_m &= e_m^+ + e_m^- = e_m^+ + \frac{q_m^-}{c_{gm} S_m} = e_m^+ + \frac{1}{c_{gm} S_m} (r_{mm} q_m^+ + \tau_{nm} q_n^-) \\ &= (1 + r_{mm})\, e_m^+ + \frac{c_{gn} S_n}{c_{gm} S_m} \tau_{nm} e_n^-, \end{aligned} \tag{10}$$

where c_{gm} is the group speed of the left member and c_{gn} the group speed of the right member. In a similar manner the energy density at the connection of the right long member with the short member can be written as

$$e_n = \frac{c_{gm} S_m}{c_{gn} S_n} \tau_{mn} e_m^+ + (1 + r_{nn}) e_n^-. \tag{11}$$

Combining equations (10) and (11) in matrix from results in

$$\begin{Bmatrix} e_m \\ e_n \end{Bmatrix} = \begin{bmatrix} (1 + r_{mm}) & \dfrac{c_{gn} S_n}{c_{gm} S_m} \tau_{nm} \\ \dfrac{c_{gm} S_m}{c_{gn} S_n} \tau_{mn} & (1 + r_{nn}) \end{bmatrix} \begin{Bmatrix} e_m^+ \\ e_n^- \end{Bmatrix} = [E] \begin{Bmatrix} e_m^+ \\ e_n^- \end{Bmatrix}. \tag{12}$$

The values for e_m and e_n are computed by the EFEA analysis for the long members. In the EFEA analysis, the power transfer coefficients at joints with short members capture the resonant behavior and the dissipation occurring in the short members. The values for e_m^+ and e_n^- are computed by equation (12), and they are utilized to prescribe the excitation on the short member. Only the component of the energy density associated with the wave impinging on the short member is employed for defining the excitation on the short member. The excitation applied from each long member on the short is considered as

incoherent because it originates from the reverberant field of each long member. The energy densities e_m^+ of the impinging wave from the left semi-infinite member can be associated with the amplitude of the wave as

$$e_m^+ = \tfrac{1}{2}\rho_m \omega^2 |A_m^m|^2 . \tag{13}$$

Equations (7) and (13) are employed for developing relationships between the FEA primary variables at the two ends of the short member and the amount of energy density associated with the impinging wave at the joint,

$$u_m^m = a_1^m A_m^m, \quad \mathrm{d}u_m^m/\mathrm{d}x = a_2^m A_m^m, \quad u_n^m = a_3^m A_m^m, \quad \mathrm{d}u_n^m/\mathrm{d}x = a_4^m A_m^m. \tag{14}$$

The relative phase information within the short member is retained in the computations because the constants a_i^m have complex values. In a similar manner, by considering the impinging wave from the right semi-infinite member, a set of relationships can be developed between the EFEA energy density associated with the impinging wave at the edge of the right long member at the joint and the FEA primary variables at the two ends of the short member.

When the excitation is considered to be applied on long members the global EFEA system matrix is assembled for all of the long members. The power transfer coefficients derived by the hybrid joint formulation between short and long members are employed for developing the joint matrices $[JC]_j^i$ for long members connected through short ones. The EFEA system of equations is solved first. The distribution of the energy density over all of the long members is evaluated. Equations (13) and (14) are employed for identifying appropriate boundary conditions on each short member of the system due to the distribution of the energy density on the long ones. Each short member is subjected to incoherent excitation from the presence of a certain amount of energy density at every interface with a long member. Since the excitations e_m and e_n are incoherent, the total response and the energy density distribution over the short members is evaluated by adding the responses on an energy basis. The effects from power re-injection and power re-radiation are accounted in the solution because equation (12) includes, in matrix $[E]$, terms associated with both power reflected from the joint and power transmitted from the other long member. The computation of the total response is equivalent to a random analysis of a linear system subjected to incoherent excitation, i.e., no cross-correlation terms exist between excitation applied at different positions [24]. This concludes the overview of the hybrid FEA formulation that is utilized in the investigation of power flow presented in this paper.

3. DERIVATION OF ENERGY VARIABLES FOR A SHORT MEMBER

In order to investigate power flow concepts, energy variables must be computed for both long and short members. In the hybrid FEA the long members are modelled by the EFEA and the energy density constitutes the primary variable. Thus, energy variables are readily available for the long members. The short members are modelled by the conventional FEA method, therefore, energy variables must be computed from the FEA primary variables of the short members. The derivation of energy variables from the FEA results and the FEA shape functions is presented in this section.

The time-averaged energy density for flexural waves in a beam is

$$\langle e \rangle = \frac{1}{4}\frac{EI}{S}\left\{\frac{\partial^2 U}{\partial x^2}\left(\frac{\partial^2 U}{\partial x^2}\right)^*\right\} + \frac{1}{4}\rho\left\{\frac{\partial U}{\partial t}\left(\frac{\partial U}{\partial t}\right)^*\right\}, \tag{15}$$

where S is the cross-sectional area, ρ the density, and $U = u(x)\,e^{i\omega t}$ the harmonic displacement solution. The products of equation (15) can be expressed in terms of only the space-dependent displacement solution:

$$\frac{\partial^2 U}{\partial x^2}\left(\frac{\partial^2 U}{\partial x^2}\right)^* = \frac{d^2 u}{dx^2}\left(\frac{d^2 u}{dx^2}\right) = \left|\frac{d^2 u}{dx^2}\right|^2, \tag{16}$$

$$\frac{\partial U}{\partial t}\left(\frac{\partial U}{\partial t}\right)^* = \omega^2 uu^* = \omega^2 |u|^2. \tag{17}$$

The equation for the energy density can be simplified further as

$$\langle e\rangle = \frac{1}{4}\frac{EI}{S}\left|\frac{d^2 u}{dx^2}\right|^2 + \frac{1}{4}\rho\omega^2 |u|^2. \tag{18}$$

In FEA the displacement function for a beam element can be expressed in terms of the primary variables at the nodes (u_1, du_1/dx, u_2, du_2/dx) and in terms of the shape functions ($N1$, $N2$, $N3$, $N4$). Therefore, the second derivative of the displacement can also be expressed in terms of the nodal variables and the second derivatives of the shape functions with respect to space.

The energy density can be expressed in terms of the shape functions, derivatives of the shape functions, and the FEA primary variables at the nodes,

$$\langle e\rangle = \frac{1}{4}\frac{EI}{S}\left|\frac{d^2 N1}{dx^2}u_1 + \frac{d^2 N2}{dx^2}\frac{du_1}{dx} + \frac{d^2 N3}{dx^2}u_2 + \frac{d^2 N4}{dx^2}\frac{du_2}{dx}\right|^2$$

$$+ \frac{1}{4}\rho\omega^2\left|N1u_1 + N2\frac{du_1}{dx} + N3u_2 + N4\frac{du_2}{dx}\right|^2. \tag{19}$$

Therefore, the energy density can be evaluated at any point of the short members.

In order to demonstrate that the energy density calculations based on FEA results provide the correct energy values for a short number, a single beam is analyzed by FEA and the energy density solutions are compared between analytical solutions and FEA results. The one-beam system (Figure 1) has free–free boundary conditions and is subjected to a point force excitation at the left end. The properties of the beam are the same as the properties of the short member listed in Table 2. The energy density solutions computed by analytical and FEA methods are presented in Figure 2. The short beam is comprised of 40 finite elements. The analytical and FEA solutions correlate well with each other.

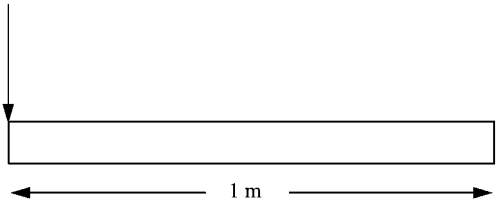

Figure 1. Single-beam system.

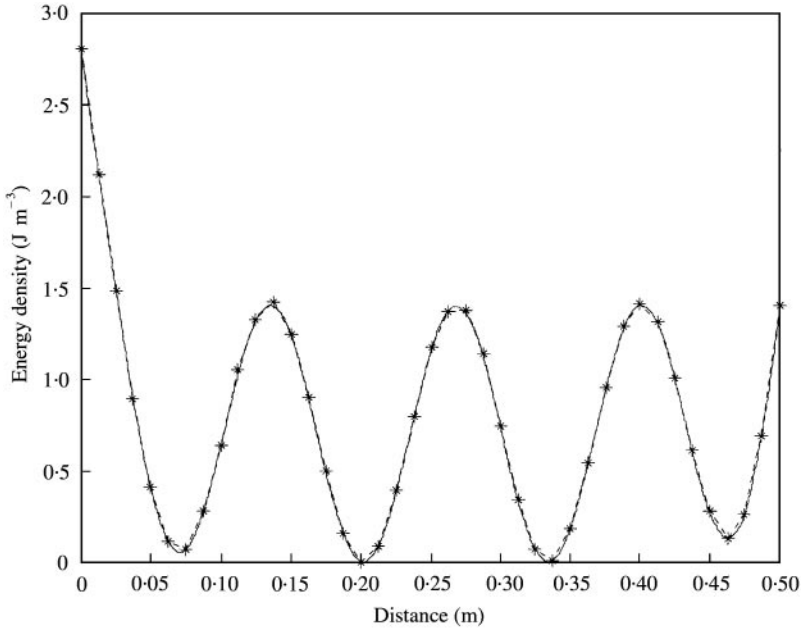

Figure 2. Analytical and FEA results for energy density in single-beam system: ——, analytical; —✶—, FEA.

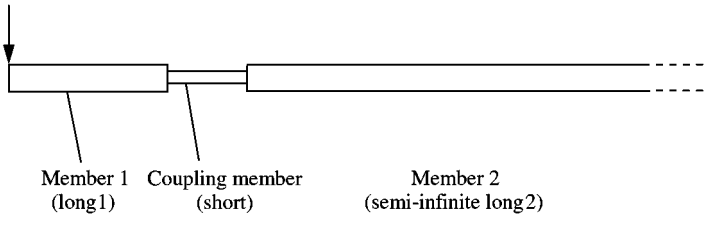

Figure 3. Three-beam assembly in system A.

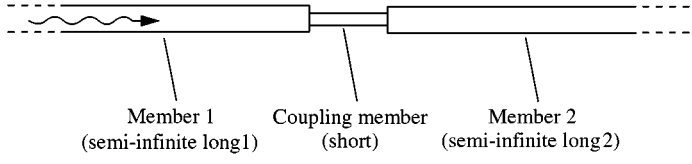

Figure 4. Three-beam assembly in system B.

4. INVESTIGATION OF POWER FLOW

A system of three co-linear beams is utilized in all the power flow investigations. The middle beam always constitutes a short member while the other two are long members. The flexural and damping properties and the dimensions of the beams vary depending on the power flow concept that is investigated. Figures 3–6 present all the configurations employed in the analyses and Tables 1–5 summarize the properties of the members in the different systems. Analytical solutions that assign a 4% uncertainty [26] in the dimensions of the

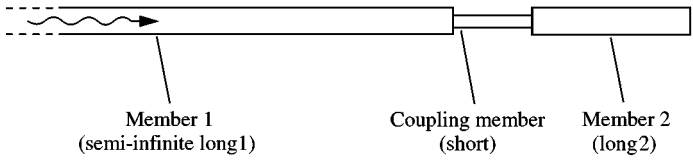

Figure 5. Three-beam assembly in system C.

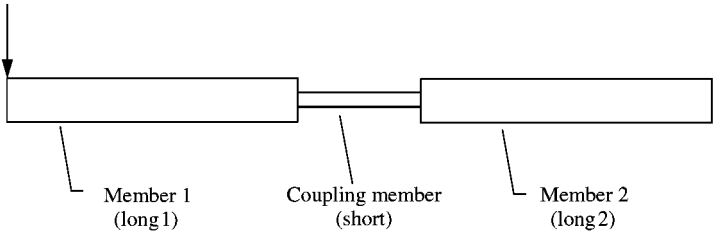

Figure 6. Three-beams assembly utilized in systems D–F.

TABLE 1

Configurations of the systems employed in the analyses

Length of members (m)	Member 1	Coupling member	Member 2
System A	3	0·5	Semi-infinite
System B	Semi-infinite	0·5	Semi-infinite
System C	Semi-infinite	0·5	3
Systems D–G	3	0·5	3

TABLE 2

Properties of beams employed in systems A–C

	Long member/ semi-infinite member	Short member
Young's modulus of elasticity E (N/m^2)	$19{\cdot}5 \times 10^{10}$	$19{\cdot}5 \times 10^{10}$
Moment of inertia I (m^4)	$9{\cdot}365 \times 10^{-10}$	$5{\cdot}853 \times 10^{-11}$
Mass density ρ (kg/m^3)	7700	7700
Damping factor η	0·02 (Long members) 0·0 (Semi-infinite members)	0·02
Cross-sectional area A (m^2)	$1{\cdot}935 \times 10^{-4}$	$0{\cdot}4839 \times 10^{-4}$
Cross-sectional dimensions width × height (m)	$0{\cdot}0254 \times 0{\cdot}00762$	$0{\cdot}0127 \times 0{\cdot}00381$

long members are presented along with the hybrid FEA results in order to validate the computations. The following power flow concepts are investigated: (1) power re-injection; (2) power re-radiation; (3) effects of the coupling damping on the power transferred between long members; (4) effects of the coupling rigidity on the power transferred between long members; (5) control of power flow between long members by appropriate selection of

TABLE 3

Properties of beams employed in system D

	Long member	Short member
Young's modulus of elasticity E (N/m^2)	$19{\cdot}5 \times 10^{10}$	$19{\cdot}5 \times 10^{10}$
Moment of inertia I (m^4)	$9{\cdot}365 \times 10^{-10}$	$5{\cdot}853 \times 10^{-11}$
Mass density ρ (kg/m^3)	7700	7700
Damping factor η	0·02	0·0–0·5
Cross-sectional area A (m^2)	$1{\cdot}935 \times 10^{-4}$	$0{\cdot}4839 \times 10^{-4}$
Cross-sectional dimensions width × height (m)	$0{\cdot}0254 \times 0{\cdot}00762$	$0{\cdot}0127 \times 0{\cdot}00381$

TABLE 4

Properties of beams employed in system E

	Long member	Short member
Young's modulus of elasticity E (N/m^2)	$19{\cdot}5 \times 10^{10}$	$19{\cdot}5 \times 10^{10}$
Moment of inertia I (m^4)	$9{\cdot}365 \times 10^{-10}$	$4{\cdot}741 \times 10^{-13}$ – $6{\cdot}145 \times 10^{-10}$
Mass density ρ (kg/m^3)	7700	7700
Damping factor η	0·02	0·02
Cross-sectional area A (m^2)	$1{\cdot}935 \times 10^{-4}$	$4{\cdot}355 \times 10^{-6}$ – $1{\cdot}568 \times 10^{-4}$
Cross-sectional dimensions width × height (m)	$0{\cdot}0254 \times 0{\cdot}00762$	$0{\cdot}0038 \times 0{\cdot}00114$ – $0{\cdot}0229 \times 0{\cdot}0069$

TABLE 5

Properties of beams employed in system F

	Long member	Short member
Young's modulus of elasticity E (N/m^2)	$19{\cdot}5 \times 10^{10}$	$19{\cdot}5 \times 10^{10}$
Moment of inertia I (m^4)	$9{\cdot}365 \times 10^{-10}$	$1{\cdot}405 \times 10^{-11}$
Mass density ρ (kg/m^3)	7700	7700
Damping factor η	0·02	0·05
Cross-sectional area A (m^2)	$1{\cdot}935 \times 10^{-4}$	$0{\cdot}2371 \times 10^{-4}$
Cross-sectional dimensions width × height (m)	$0{\cdot}0254 \times 0{\cdot}00762$	$0{\cdot}0089 \times 0{\cdot}0027$

coupling damping and coupling rigidity for the short member; (6) sensitivity of the power transferred between long members with respect to the coupling damping ratio and the relative rigidity exhibited by the long members.

4.1. POWER RE-INJECTION

The phenomenon of power re-injection occurs at a joint between a finite source member and a receiving member. Power reflected from the joint back into the finite source member

is later incident upon the joint and eventually partly transmitted to the receiving member. In references [19, 21] an analytical solution for two continuous one-dimensional subsystems was utilized to demonstrate that the power flow per unit power input from a finite to an infinite subsystem is always greater than that between two infinite subsystems due to the re-injection of power by the finite source subsystem. The hybrid FEA can account for power re-injection effects since it is a wave-based formulation and the excitation applied on a short member depends only on the waves impinging from the adjacent long members [Equation (12)–(14)]. In order to demonstrate the presence of the power re-injection effect in the hybrid FEA solution two systems are analyzed. System A is comprised of a long member coupled to a semi-infinite member through a short member (Figure 3). System B is comprised of two semi-infinite members coupled through a short member (Figure 4). No damping is applied to the two semi-infinite members and a nominal damping of $\eta = 0{\cdot}02$ is applied to the short member. The hybrid FEA and an analytical solution are utilized for modelling system A while an analytical solution only is employed for modelling system B. The properties of the two systems are summarized in Tables 1 and 2. The bending rigidity is the same for all long and semi-infinite members in systems A and B, and the same short member is utilized in systems A and B.

Input power is applied as excitation at the left end of the left long member of system A. A right-travelling wave defines the excitation on the left semi-infinite member of system B. In order to perform a proper comparison, the external input power into system A is equal to the power of the right-travelling wave in the left semi-infinite member of system B. Calculations are performed in the frequency range of 200–1000 Hz. In the selected frequency range the long and the short member of system A contain more than six and less than six wavelengths, respectively, while uncertainty effects are only considered for the long members. The results for the normalized power flow per unit of input power from the left long member to the short member in system A, and the normalized power flow per unit of input power from the left semi-infinite member to the short member in system B are presented in Figure 7. The power flow is computed at the joint between the left long member and the short member in system A and at the joint between the left semi-infinite member and the short member in a system B. The time-averaged power flow for flexural waves in a beam is

$$\langle q \rangle = \frac{EI}{2} \operatorname{Re} \left\{ \left(\frac{\partial^3 U}{\partial x^3} \right) \left(\frac{\partial U}{\partial t} \right)^* + \left(\frac{\partial^2 U}{\partial x^2} \right) \left(- \frac{\partial^2 U}{\partial x \, \partial t} \right)^* \right\}. \tag{20}$$

Both the hybrid and the analytical solutions are presented for system A. In the hybrid FEA solution the semi-infinite receiving member of system A is modelled by a very long finite member (300 m) with very high damping ($\eta = 0{\cdot}9$) in order to eliminate possible power reflection from the edge of the receiving member. In the analytical solution for system A the receiving member is modelled as semi-infinite and no reflection occurs. As expected, power is re-injected back towards the joint when the length of the source member is finite, and the power flow towards the short member is higher compared to the power flow when the source member is semi-infinite. In system A, almost the entire part of the input power (other than the amount dissipated in the finite left long member) is transferred to the receiving semi-infinite member. Thus, the normalized power flow per unit of input power is very close to unit. The differences between systems A and B are amplified at frequencies where the power flow associated with the reflected wave presents peaks. Then, the power transferred to the receiving long member is significantly higher in system A compared to system B due to the power re-injection effect. The hybrid FEA and the analytical results for system A correlate very well over the entire frequency range of analysis.

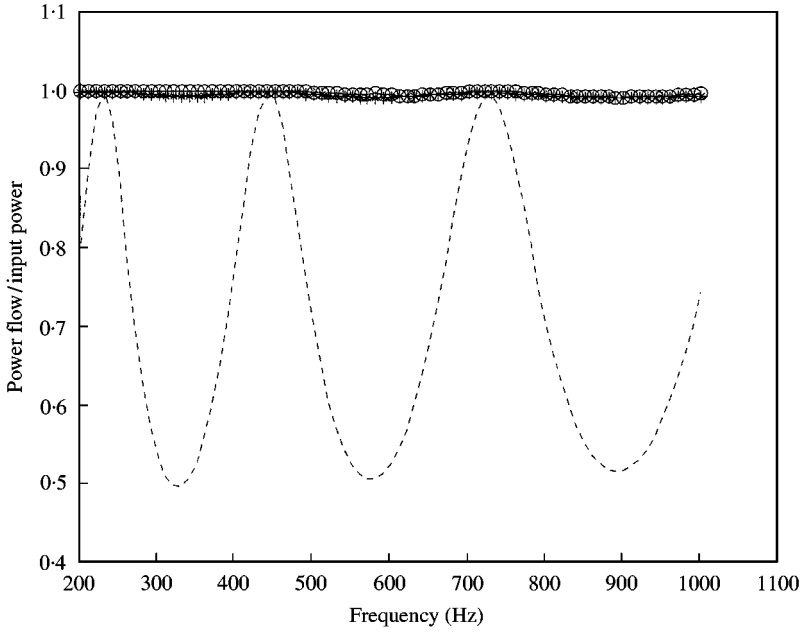

Figure 7. Ratio of power transferred to the receiving semi-infinite member over the input power for simulations demonstrating power re-injection effects: —✶—, analytical system A; —○—, hybrid system A; – – –, analytical system B.

4.2. POWER RE-RADIATION

Power re-radiation occurs when some of the power radiated to a finite receiving member is re-radiated back to the source member. In references [19, 21] an analytical wave solution for power flow between two continuous one-dimensional subsystems was used to investigate the phenomenon of power re-radiation. It was demonstrated that the power flow per unit of external input power from a semi-infinite to a finite subsystem is always smaller than the power flow between two semi-infinite subsystems due to the power re-radiated back to the source semi-infinite member by the finite receiving member. The power re-radiation phenomenon is accounted in the hybrid FEA. In order to demonstrate the effect of power re-radiation, analyses are performed on two systems. System C is comprised of a semi-infinite member coupled with a long finite member through a short member (Figure 5). System B is the one utilized in the previous section. The hybrid FEA and an analytical solution are employed for analyzing system C. In the hybrid solution the semi-infinite source member of system C is modelled by a very long finite member (300 m). High damping ($\eta = 0{\cdot}9$) is assigned to the first 297 m of the source member and nominal damping ($\eta = 0{\cdot}02$) is assigned to the 3 m closest to the joint with the short member. The external input power is applied at the point where the damping changes values. The power of the impinging wave from the source member to the joint with the short member in system C is retained equal with the power of the right travelling wave in the source semi-infinite member of system B. Thus, the power impinging from the source member to the short member is the same for both system. In the analytical solution for system C the source member is modelled as semi-infinite with no damping, and the input power is specified similar to system B. An analytical solution computes the response of system B. No damping is defined on the semi-infinite members and nominal damping ($\eta = 0{\cdot}02$) is defined for the

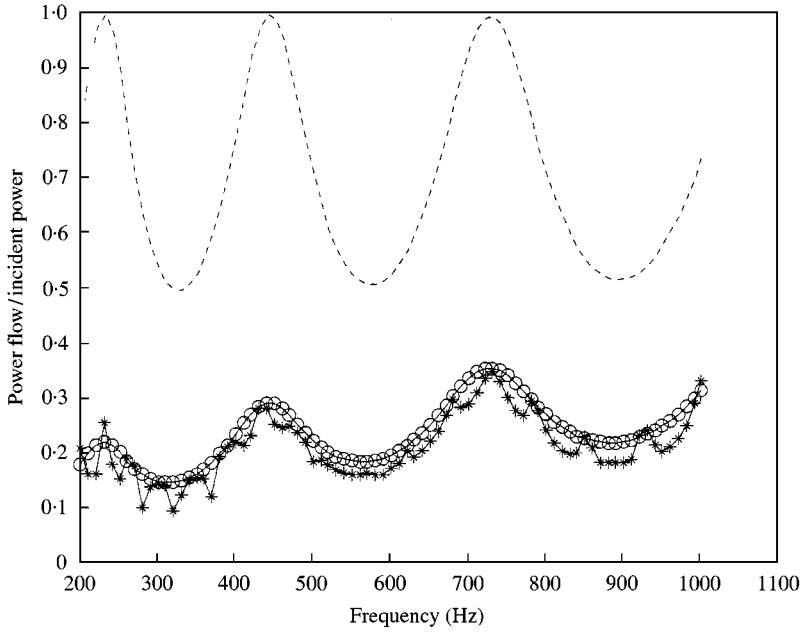

Figure 8. Ratio of power transferred to the receiving member over the incident power for simulations demonstrating power re-radiation effects: —✶—, analytical system C; —○—, hybrid system C; – – –, analytical system B.

short member. The properties of system C are summarized in Tables 1 and 2. The net normalized power flow per unit of incident power from the left semi-infinite member to the short member is calculated over the frequency range 200–1000 Hz and the results are presented in Figure 8. The results for system B are identical with the result presented in Figure 7, since the configuration of System B remains the same during the power re-injection and the power re-radiation analyses. Although the power of the impinging wave at the joint between the source and the short member is the same for systems B and C, the net power flow at the joint is not the same due to the re-radiation phenomenon. The net power flow to the short member is always lower in system C than that in system B. The reason for the lower power flow exhibited in system C is that power is re-radiated back into the source member from the right boundary of the finite receiving long member. In system B, the receiving long member is a semi-infinite one, therefore power is not reflected back into the source member. The power receiving mechanism in the system B presents higher capacity than in system C due to the semi-infinite nature of the receiving long member. Good correlation can be observed between the hybrid FEA and analytical results over the frequency range of analysis.

4.3. COUPLING DAMPING

The effect of coupling damping is investigated in a system comprised by two long beams inter-connected by a short one (system D). Excitation is applied at the left end of the left long member and the effect of the structural damping of the short beam to the power transferred between the two long members is identified. In the past, the power flow between two non-conservatively coupled oscillators was studied, and the effect of the coupling damping to the power flow was determined [22, 23]. In this paper, two continuous long

members are employed instead of oscillators and the connecting short member comprises the non-conservative coupling mechanism. The structural damping η of each member defines its dissipation characteristics. A relationship between the damping coefficient c of a non-conservative oscillator and the structural damping coefficient of a continuous member utilized in this work can be derived as

$$c\omega = (EI)\eta, \tag{21}$$

where ω is the radial frequency, and EI the bending rigidity. This relationship can be employed for comparing quantitatively outcomes between this work and references [22], [23]. The properties of system D are listed in Tables 1 and 3. The damping of the coupling short member is considered as a varying parameter and the energy stored in the beams is evaluated. The structural damping of the short member η_S varies from 0·0 to 0·5. The two long members are considered to demonstrate the same amount of structural damping, equal to 0·02. By considering resonance with 3 dB bandwidth, the modal overlap can be computed as [27]

$$M = \frac{\omega L \eta}{c_B \pi}, \tag{22}$$

where M is the modal overlap, L the length of member, and c_B the bending wave speed. The modal overlap for the long members utilized in system D acquires values between 0·3 and 0·34 in the frequency range of analysis. The modal overlap for the short member acquires values between 0 and 4·012 depending primarily on the value of structural damping and to a lesser extent on the frequency. The modal overlap for the short member reaches the value

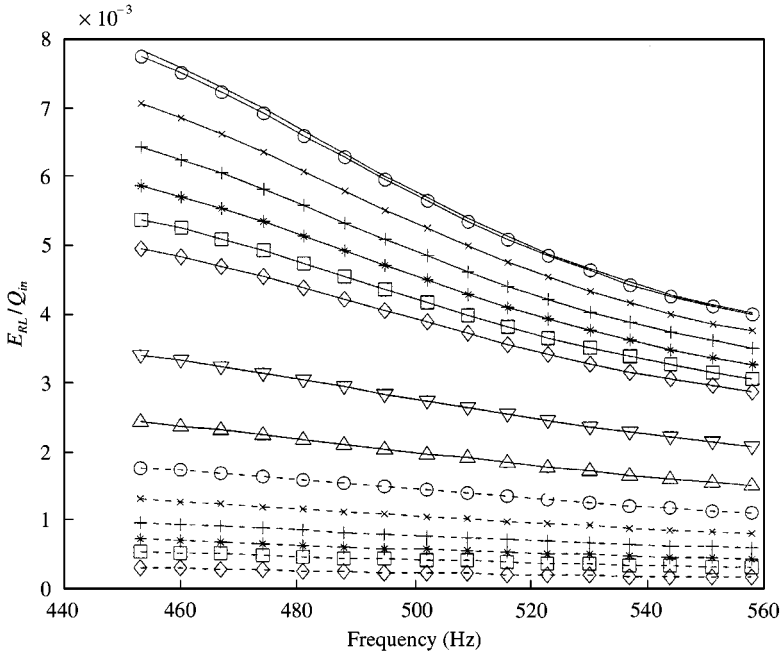

Figure 9. Hybrid results for the total energy in the receiving long member per unit of external input power in system D: ——, $\eta_S = 0{\cdot}0$; —○—, 0·001; —×—, 0·01; —+—, 0·02; —✳—, 0·03; —□—, 0·04; —◇—, 0·05; —▽—, 0·1; —△—, 0·15; – ⊖ –, 0·2; – – × – –, 0·25; – – + – –, 0·3; ··✳··, 0·35; – ⊟ –, 0·4; – ◇ –, 0·5.

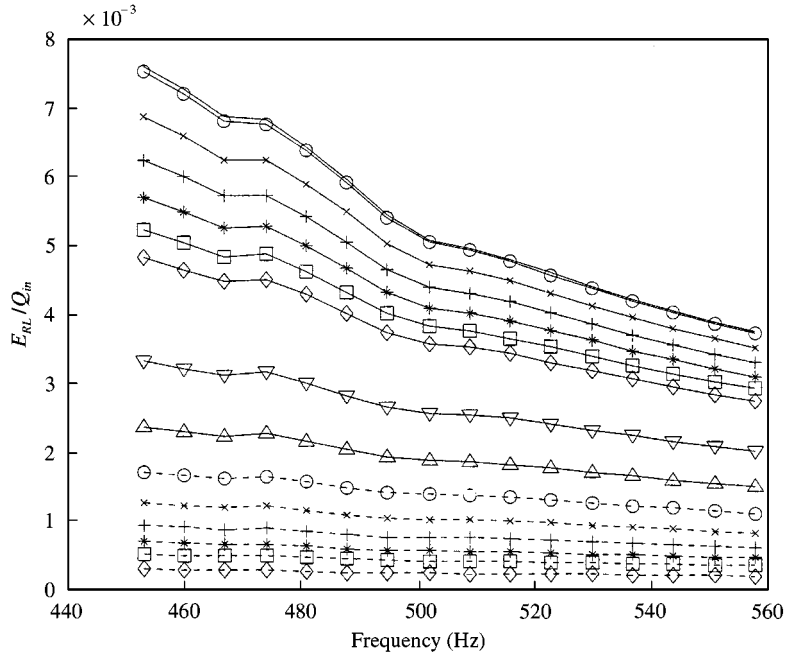

Figure 10. Analytical results for total energy in the receiving long member per unit of external input power in system D: ——, $\eta_S = 0{\cdot}0$; —○—, 0·001; —×—, ,0·01; —+—, 0·02; —✶—, 0·03; —□—, 0·04; —◇—, 0·05; —▽—, 0·1; —△—, 0·15; – ⊖ –, 0·2; – –×– –, 0·25; – – + – –, 0·3; ··✶··, 0·35; — □ —, 0·4; – ◇ –, 0·5.

of 0·3, the same as exhibited by the long members, for structural damping of 0·05. Results for the energy stored in the receiving long member (E_{RL}) per unit of external power input are presented in Figures 9 and 10 from the hybrid FEA and the analytical solutions respectively. The hybrid FEA can account for the coupling damping since the FEA model of the coupling short member takes into account the dissipation characteristics of the short member.

The following characteristics can be observed for the power transferred between the two long members: (1) overall, the total energy of the receiving long member per unit of external input power decreases when the coupling damping increases. (2) For high values of coupling damping there is a progressively smaller influence on the energy stored in the receiving long member. These observations are in agreement with conclusions from references [22, 23]. Good correlation is observed between the hybrid FEA and the analytical results for all analyses. Both the magnitude of the energy stored in the receiving long member, and effects of the coupling damping on the results are predicted correctly by the hybrid FEA. Figure 11 presents a comparison between hybrid FEA and EFEA results for the energy stored in the receiving long member per unit of external power input. The EFEA constitutes a typical high-frequency method and the comparison is presented in order to demonstrate the benefits offered by the hybrid FEA. Results are compared for four damping values assigned to the short member (0·001, 0·02, 0·05, and 0·1). The corresponding ranges for the modal overlap values of the short member are, respectively, 0·0072–0·008, 0·144–0·16, 0·3597–0·4012, and 0·71–0·8. For the two lower values of structural damping the modal overlap factor of the short member is significantly lower than the modal overlap of the two long members, and the differences between the hybrid FEA and EFEA results are significant. For structural damping equal or larger than 0.05 the modal overlap factor of the

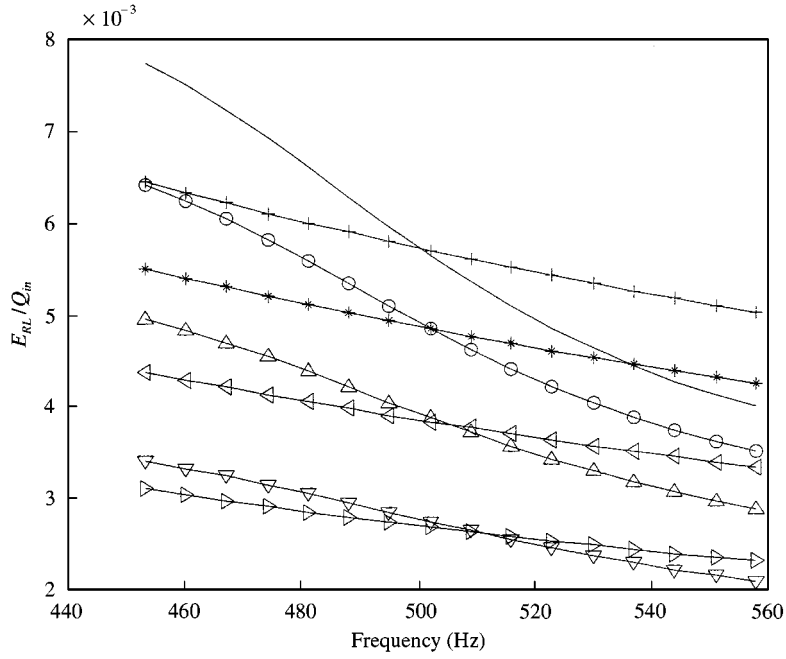

Figure 11. Comparison between hybrid FEA and EFEA results for total energy in the receiving long member per unit of external input power in system D: ——, hybrid $\eta_S = 0{\cdot}001$; —○—, hybrid $\eta_S = 0{\cdot}02$; —△—, hybrid $\eta_S = 0{\cdot}05$; —▽—, hybrid, $\eta_S = 0{\cdot}1$; —+—, EFEA $\eta_S = 0.001$; —✶—, EFEA $\eta_S = 0{\cdot}02$; —◁—, EFEA $\eta_S = 0{\cdot}05$; —▷—, EFEA $\eta_S = 0{\cdot}1$.

short member becomes of the same magnitude or higher than the modal overlap factor of the long members and the two solutions start to converge. Differences exist between the two solutions, even for values of modal overlap for the short member between 0.3597 and 0.4012 ($\eta = 0.05$), since the mid-frequency effects are a combination of the modal overlap factor and the relative magnitude between the dimension of a member and the corresponding wavelength. Although higher damping increases the modal overlap factor of the short member, the relative long wavelength with respect to the dimension of the short member allows the system to retain resonant characteristics. As the damping of the short member increases further, these resonant characteristics diminish, and the two solutions converge.

In the system of the two non-conservatively coupled oscillators it was identified that the progressively smaller influence of the coupling damping on the energy of the receiving oscillator occurs when the coupling damping exceeds the damping of the oscillators [22, 23]. In order to compare this observation with the current results, equivalent damping coefficients for the beams of system D are evaluated from equation (2). The effect of coupling damping on reducing the energy level of the receiving member is expected to become progressively smaller when the damping coefficient of the short member c_s exceeds the maximum damping coefficient of the long members ($c_S > \max(c_{SL}, c_{RL})$). Subscripts "*S*", "*SL*", and "*RL*" indicate, respectively the short, the source long, and the receiving long members (Figure 12). By taking into account the bending rigidity of the members and their structural damping, the corresponding relationship between the structural damping factors of the members in $\eta_S > 16 \max(\eta_{SL}, \eta_{RL})$. The progressively smaller effect of the coupling damping in the reduction of the energy level in the indirectly driven long member is expected to appear when η_S exceeds the value of 0·32. In order to investigate the

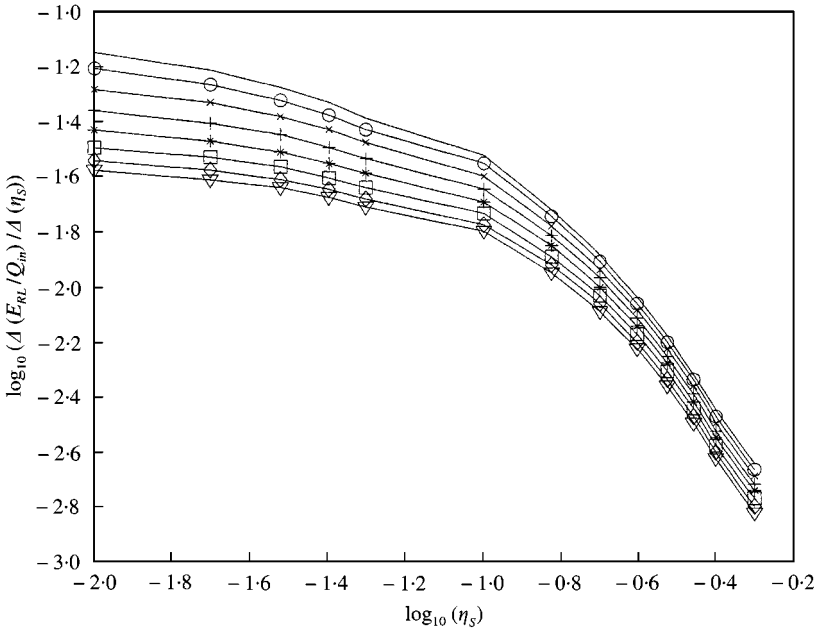

Figure 12. Reduction in the energy of the receiving long member with respect to the coupling damping; ——, Frequency = 460 Hz; —○—, 474 Hz; —×—, 488 Hz; —+—, 502 Hz; —✳—, 516 Hz; —□—, 530 Hz; —◇—, 544 Hz; —▽—, 558 Hz.

progressively smaller influence of the coupling damping on the energy of the receiving member, the ratio of the change in the energy of the receiving member over the change in the coupling damping is plotted in a logarithmic scale with respect to the coupling damping value. It can be observed, that the decline in the curve becomes steeper for damping values of $\log_{10}(\eta_S)$ equal to $-0{\cdot}6$ ($\eta_S = 0{\cdot}25$) and higher. The steep decline in the curve indicates that the energy stored in the receiving long member is influenced minimally by the increase of the coupling damping. Thus, the trend remains similar to the observations made in references [22], [23].

Overall, the total energy in the receiving long member per unit of external input power decreases when the coupling damping increases. The coupling damping provides a dissipation mechanism for the system. Due to the resonant characteristics of the short member, power is dissipated before it is transferred to the receiving long member. Therefore, the amount of coupling damping impacts the power flow between the long members and the amount of energy stored in the indirectly driven long member. The hybrid FEA can be utilized in the mid-frequency range for determining the impact of the coupling damping in the isolation of the receiving member.

4.4. COUPLING RIGIDITY

The bending rigidity of the coupling short member in system D is considered as a parameter in order to investigate the effect of the coupling rigidity on the power flow of the system in the mid-frequency range. The short member exhibits resonant behavior in the mid-frequency range. Therefore, the energy stored in the short member per unit of external input power will become maximum for the value of coupling bending rigidity that

introduces a resonance in the short member in the frequency range of analysis. The coupling rigidity of the short member is modified by varying the dimensions of the cross-section. The width and the height of the cross-section of the short member are modified simultaneously by the same percentage of the baseline value. The beam system that includes the modifications for the coupling stiffness is considered as system E. The parameter ratio *rd* is defined as the ratio between the width or the height of the cross-section with respect to the corresponding baseline value. The bending rigidity of the short member takes values that are less, equal, or larger than the baseline bending rigidity of the short member. Analysis is performed in the frequency range 450–560 Hz. The modal overlap factor for the short member acquires values between 0·107 and 0·164 for all the combinations of *rd* and frequency of analysis. Therefore, the modal overlap value of the short member is substantially lower from the modal overlap values of the long members for all the configurations. The external power input is retained constant over the entire frequency range of analysis. The total energy stored in the system is computed first. Results from the hybrid FEA and the analytical computation are presented in Figures 13 and 14 respectively. The total energy stored in the system is proportional to the input power and it is expected to decrease with frequency when the input power is constant over the frequency range of analysis:

$$\langle \Pi_{diss} \rangle = \langle Q_{in} \rangle = \eta\omega \langle E_{tot} \rangle, \tag{23}$$

where $\langle \Pi_{diss} \rangle$ is the time averaged dissipated energy of the system, $\langle Q_{in} \rangle$ the time-averaged input power into the system, $\langle E_{tot} \rangle$ the time-averaged total energy in the system. From equation (23), the value of $\langle E_{tot} \rangle / \langle Q_{in} \rangle$ can be defined,

$$\frac{\langle E_{tot} \rangle}{\langle Q_{in} \rangle} = \frac{1}{\eta\omega}. \tag{24}$$

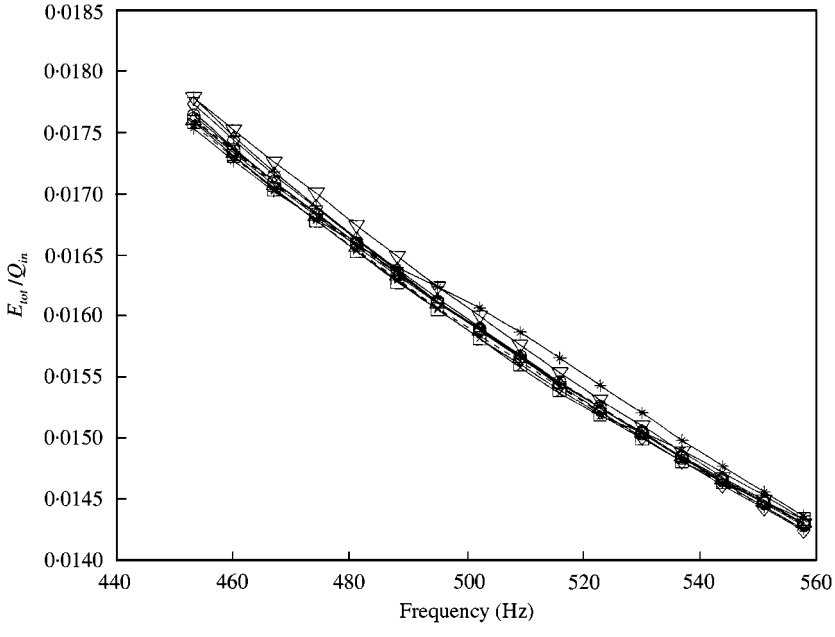

Figure 13. Hybrid results for total energy in system E per unit of external input power: ——, $rd = 0{\cdot}3$; —○—, 0·4; —×—, 0·5; —+—, 0·6; —✶—, 0·7; —□—, 0·8; —◇—, 0·9; —▽—, 1·0; —△—, 1·4; – -○- -, 1·8; – -×- -, $1/\eta\omega$.

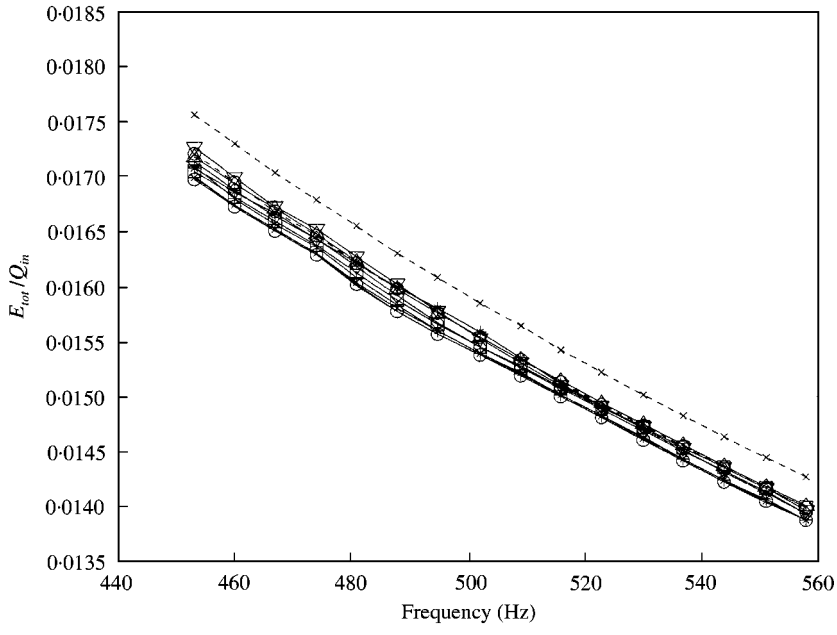

Figure 14. Analytical results for total energy in system E per unit of external input power: ——, $rd = 0{\cdot}3$; —○—, 0·4; —×—, 0·5; —+—, 0·6; —✶—, 0·7; —□—, 0·8; —◇—, 0·9; —▽—, 1·0; —△—, 1·4; —○—, 1·8; ··✶··, $1/\eta\omega$.

The curve $(1/\eta\omega)$ is plotted along with the hybrid FEA and the analytical results in Figures 13 and 14 respectively. It can be observed that conservation of energy is preserved in the hybrid FEA solution since the results for the total energy in the system agree well with the expected value derived from equation (24). The relationship between the stored and the dissipated energy defined by equation (23) is embedded in the hybrid FEA formulation. In the analytical solution the damping mechanism is introduced through a complex wave number. Therefore, equation (24) demonstrates better agreement with the hybrid FEA solution rather than the analytical results. As expected, the hybrid FEA and the analytical results for the total energy of the system per unit of external input power do not depend on the values of coupling rigidity. The total energy stored in the entire system strictly depends on the input power and the structural damping. Similar values and the same behavior is predicted in the results by both the hybrid FEA and the analytical solution.

The total energy stored in the short member is computed for different values of bending rigidity exhibited by the short member. Results computed by the hybrid FEA and an analytical solution are presented in Figures 15 and 16 respectively. The ratio parameter *rd* varies from 0·3 to 1·8. The largest amount of energy stored in the short member per unit of input power over the frequency range of analysis is exhibited for $rd = 0{\cdot}7$. This information will be employed in the next section in order to control the amount of power flow towards the receiving long member. A resonant behavior in the short member is also observed for $rd = 0{\cdot}5$. The hybrid FEA and the analytical results present good agreement. The total energy in the receiving long member per unit of external power input is computed. Results are presented in Figures 17 and 18 from the hybrid FEA and the analytical computations respectively. The amount of energy stored in the receiving long member varies significantly with respect to the coupling rigidity. The best isolation is offered when the coupling rigidity of the short member becomes very small (i.e., $rd = 0{\cdot}3$) and the two long members appear

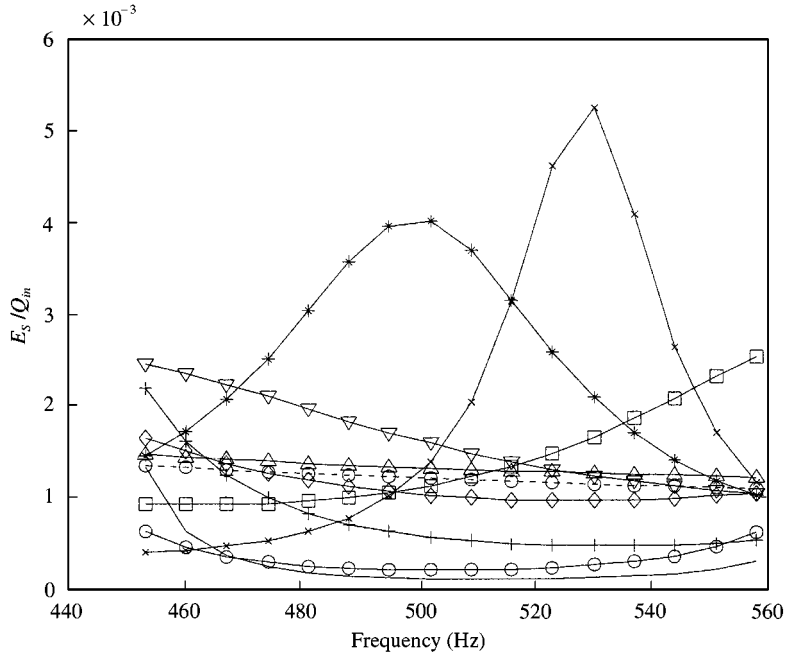

Figure 15. Hybrid results for total energy in the short member per unit of external input power in system E: ——, $rd = 0{\cdot}3$; —○—, 0·4; —×—, 0·5; —+—, 0·6; —✶—, 0·7; —□—, 0·8; —◇—, 0·9; —▽—, 1·0; —△—, 1·4; – ⊖ –, 1·8.

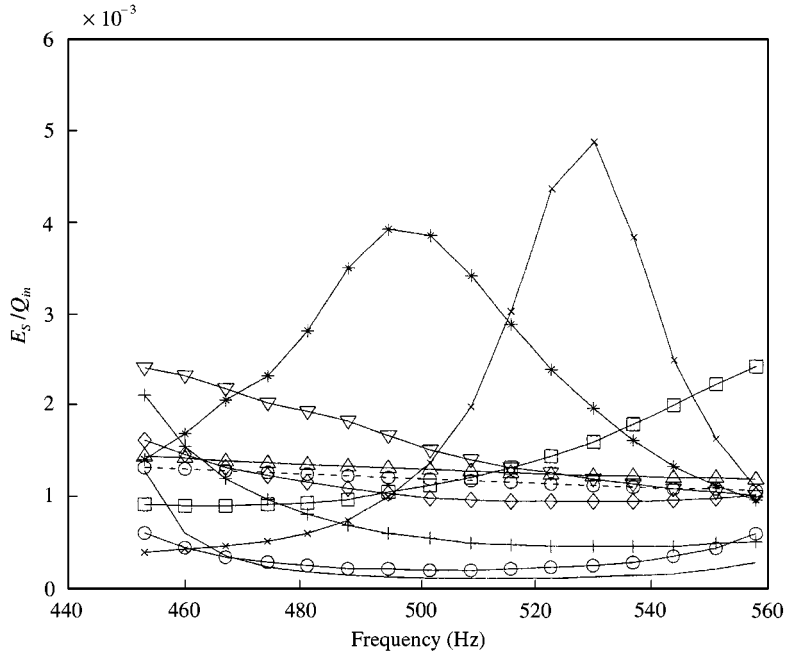

Figure 16. Analytical results for total energy in the short member per unit of external input power in system E: ——, $rd = 0{\cdot}3$; —○—, 0·4; —×—, 0·5; —+—, 0·6; —✶—, 0·7; —□—, 0·8; —◇—, 0·9; —▽—, 1·0; —△—, 1·4; —⊖—, 1·8.

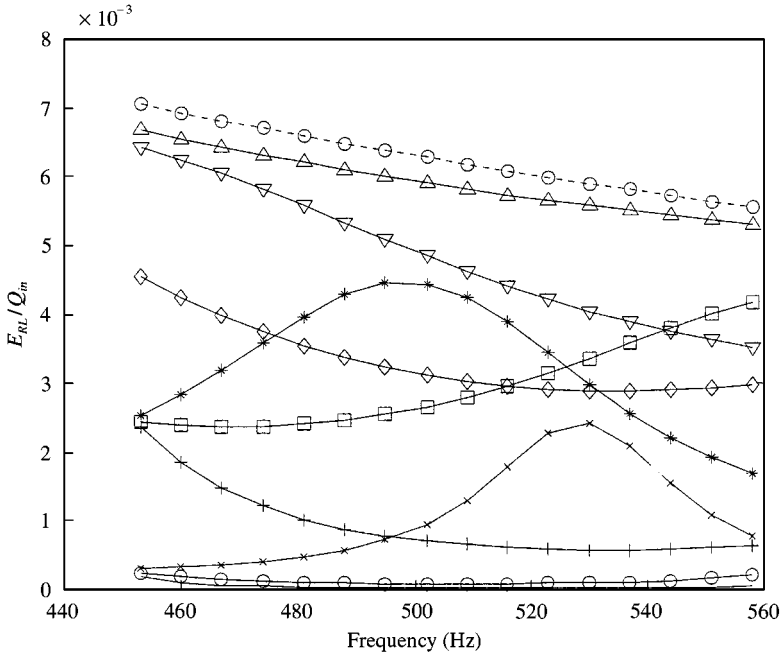

Figure 17. Hybrid results for total energy in the receiving long member per unit of external input power in system E: ——, $rd = 0{\cdot}3$; —○—, 0·4; —×—, 0·5; —+—, 0·6; —✳—, 0·7; —□—, 0·8; —◇—, 0·9; —▽—, 1·0; —△—, 1·4; —⊖—, 1·8.

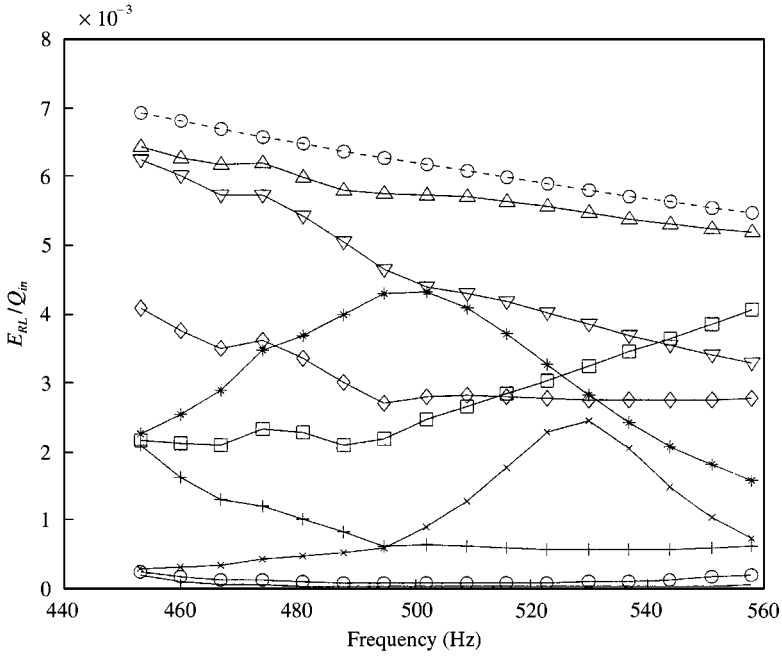

Figure 18. Analytical results for total energy in the receiving long member per unit of external input power in system E: ——, $rd = 0{\cdot}3$; —○—, 0·4; —×—, 0·5; —+—, 0·6; —✳—, 0·7; —□—, 0·8; —◇—, 0·9; —▽—, 1·0; —△—, 1·4; —⊖—, 1·8.

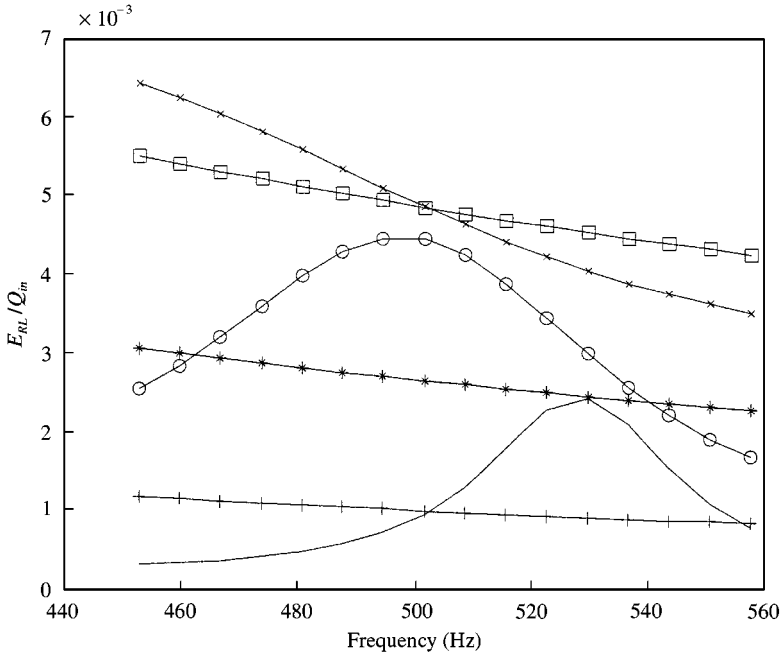

Figure 19. Hybrid FEA and EFEA results for total energy in the receiving long member per unit of external input power in system E: ——, hybrid $rd = 0{\cdot}5$; —○—, hybrid $rd = 0{\cdot}7$; —×—, hybrid, $rd = 1{\cdot}0$; —+—, EFEA $rd = 0.5$; —✶—, EFEA $rd = 0{\cdot}7$; —□—, EFEA $rd = 1{\cdot}0$.

to be disconnected. Very low values of coupling rigidity may not be acceptable due to integrity considerations.

The resonant characteristics of the short member for $rd = 0{\cdot}5$ and $0{\cdot}7$ are also present in the energy stored in the receiving long member. Good agreement is observed between the hybrid FEA and the analytical solution. Results from the hybrid FEA and the EFEA are presented in Figure 19 for three different values of coupling stiffness ($rd = 0{\cdot}5$, $0{\cdot}7$ and 1). Since the modal overlap factor of the short member is substantially lower than the modal overlap factor of the long members, there is a substantial difference between the EFEA results (that are typical of a high-frequency solution) and the hybrid FEA results. Large deviations are observed for $rd = 0{\cdot}5$ and $0{\cdot}7$ since the short member exhibits resonant behavior for these two values as it has been identified by the results presented in Figures 15 and 16.

4.5. CONTROL OF POWER FLOW BY THE COUPLING MEMBER

As it is identified in the previous two sections, the characteristics of the short member can impact the power flow to the receiving long member and the energy distribution in the system. The coupling damping and the coupling rigidity can be modified simultaneously in order to control the power flow to the receiving long member effectively. By adjusting the coupling rigidity of the short member the amount of energy stored in it can be maximized. Then, a moderate increase in the damping property of the short member will amplify the amount of dissipated energy. Thus, a lesser amount of external input power will be available to be transferred to the receiving long member. A moderate increase of structural damping

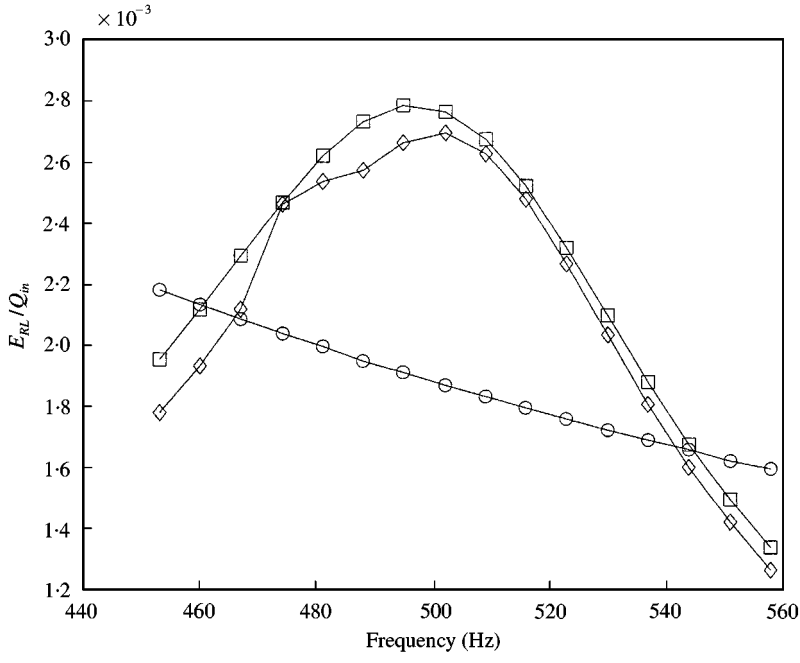

Figure 20. Analytical, hybrid FEA, and EFEA results for total energy in the receiving long member per unit of external input power in system F: —□—, hybrid; —◇—, analytical; —○—, EFEA.

(0·05 from the baseline value of 0·02) is introduced in the configuration of coupling rigidity that exhibits the highest amount of energy stored in the short member ($rd = 0{\cdot}7$) (system F). The properties of system F are summarized in Tables 2 and 5. Results computed by the hybrid FEA, an analytical solution, and the EFEA for the total energy stored in the receiving long member per unit of external power input are presented in Figure 20. The hybrid and the analytical results correlate well, while the EFEA cannot capture the resonant effects of the short member and the corresponding dissipation. By comparing the results in Figure 9 and 20 it can be observed that in order to achieve the same level of isolation with the baseline coupling stiffness the coupling damping must be increased to 20%. Also, by comparing Figure 17 and 20 it can be observed that a similar level of isolation can be achieved for the baseline structure damping only by significantly reducing the rigidity of the connecting short member. However, such an isolation measure might not be acceptable if there is a minimum rigidity requirement imposed from structural integrity considerations. Introducing a combined moderate modification in the coupling rigidity and the coupling damping can be an effective approach for reducing the power flow towards the receiving long member. An equivalent level of isolation can be achieved only by radical individual modification of the coupling stiffness or the coupling damping. Thus, the resonant behavior of the short member can be utilized in order to amplify the energy dissipated in the system and offers an isolation mechanism.

4.6. SIMULTANEOUS VARIATION OF COUPLING DAMPING AND RELATIVE RIGIDITY

The previous section addressed the importance of the properties of the coupling short member to the power flow through the system. In this section, the effects of the relative rigidity between long members and the effects of the relative damping ratio between short

TABLE 6

Properties of beams employed in system G

	Member 1	Coupling member	Member 2
Young's modulus of elasticity E (N/m^2)	$19{\cdot}5 \times 10^{10}$	$19{\cdot}5 \times 10^{10}$	$19{\cdot}5 \times 10^{10}$
Moment of inertia I (m^4)	$9{\cdot}365 \times 10^{-10}$	$5{\cdot}853 \times 10^{-11}$	$4{\cdot}683 \times 10^{-10}$–$2{\cdot}81 \times 10^{-9}$
Mass density ρ (kg/m^3)	7700	7700	7700
Damping factor η	0·02	0·02	0·02
Cross-sectional area A (m^2)	$1{\cdot}935 \times 10^{-4}$	$0{\cdot}4839 \times 10^{-4}$	$1{\cdot}369 \times 10^{-4}$ – $3{\cdot}352 \times 10^{-4}$
Cross-sectional dimensions width × height (m)	$0{\cdot}0254 \times 0{\cdot}00762$	$0{\cdot}0127 \times 0{\cdot}00381$	$0{\cdot}0214 \times 0{\cdot}00641$–$0{\cdot}0334 \times 0{\cdot}01$

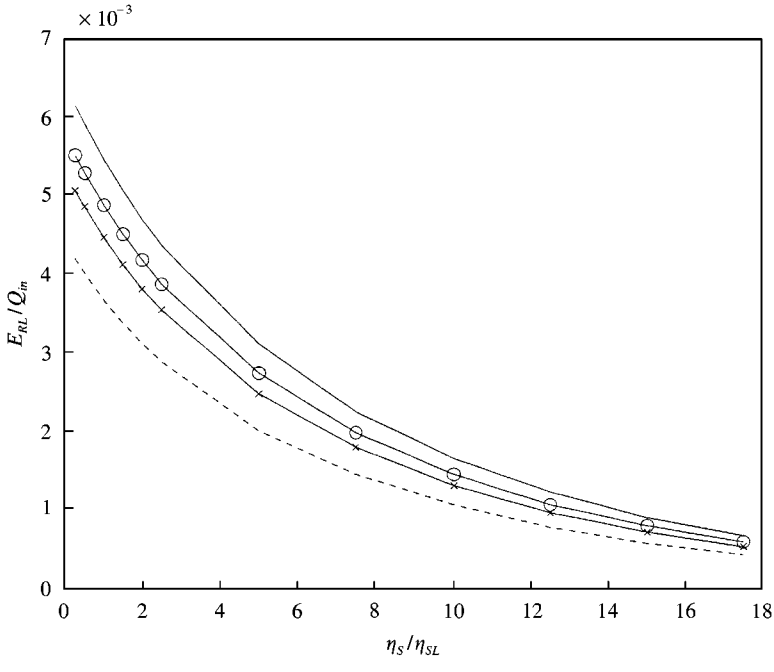

Figure 21. Hybrid results for energy stored in the receiving long member of system G: ——, $I_{RL}/I_{SL} = 0{\cdot}5$; —○—, 1·0; —×—, 1·5; – – –, 3·0.

and long members are investigated. Variations are introduced in system D and hybrid FEA analyses are performed. The system that incorporates the changes is indicated as system G and its properties are summarized in Tables 1 and 6. The parameters which are considered in the analyses are: (1) the relative rigidity between the receiving and the source long members (I_{RL}/I_{SL}), (2) the relative damping between the short and the source long member (η_S/η_{SL}). The rigidity of the receiving long member and the damping of the short member are the two parameters that vary in the system. The two parameters are modified simultaneously and the amount of total energy stored in the receiving long member per unit of external input power is computed (E_{RL}/Q_{in}). Results from the hybrid FEA and an analytical solution are presented in Figures 21 and 22 respectively. The variable E_{RL}/Q_{in} is

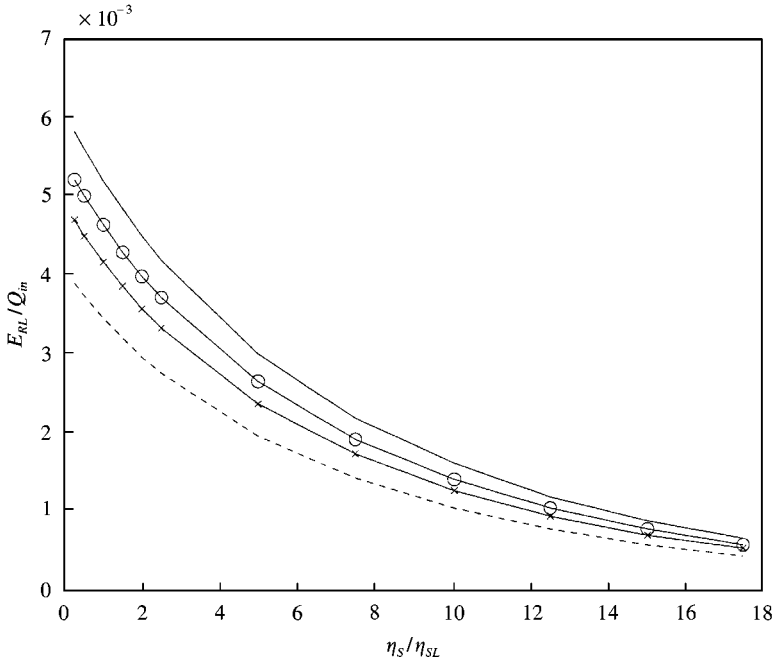

Figure 22. Analytical results for energy stored in the receiving long member of system G: ——, $I_{RL}/I_{SL} = 0{\cdot}5$; —○—, 1·0; —×—, 1·5; – – –, 3·0.

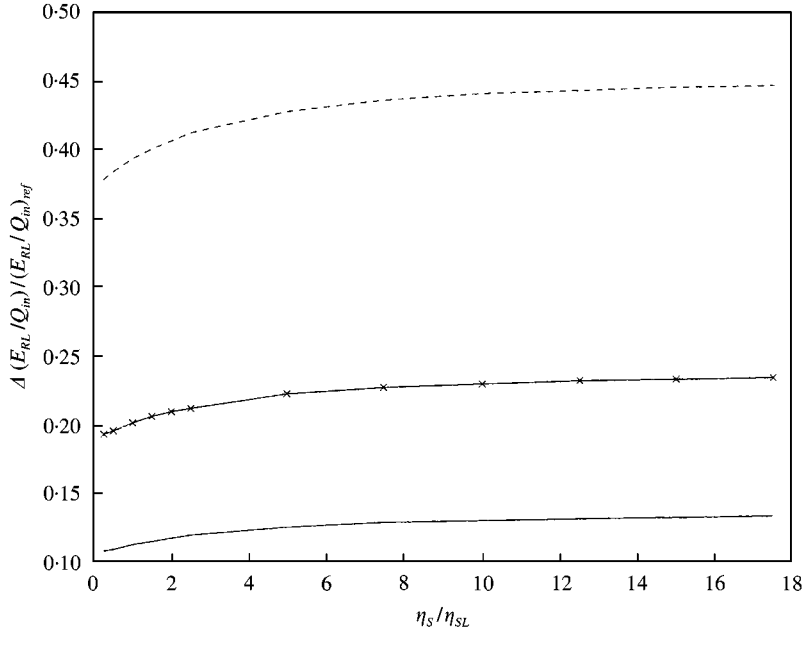

Figure 23. Hybrid results for relative variation of E_{RL}/Q_{in} with respect to I_{RL}/I_{SL} versus η_S/η_{SL} in system G: ——, $I_{RL}/I_{SL} = 0{\cdot}5$ and 1·0; —×—, 0·5 and 1·5; – – –, 0·5 and 3·0.

presented with respect to the relative damping (η_S/η_{SL}) for different values of relative rigidity (I_{RL}/I_{SL}). It can be observed (Figures 21 and 22) that the amount of energy stored in the receiving long member increases when the relative bending rigidity (I_{RL}/I_{SL}) decreases. When the receiving member becomes more flexible a larger amount of energy can be stored

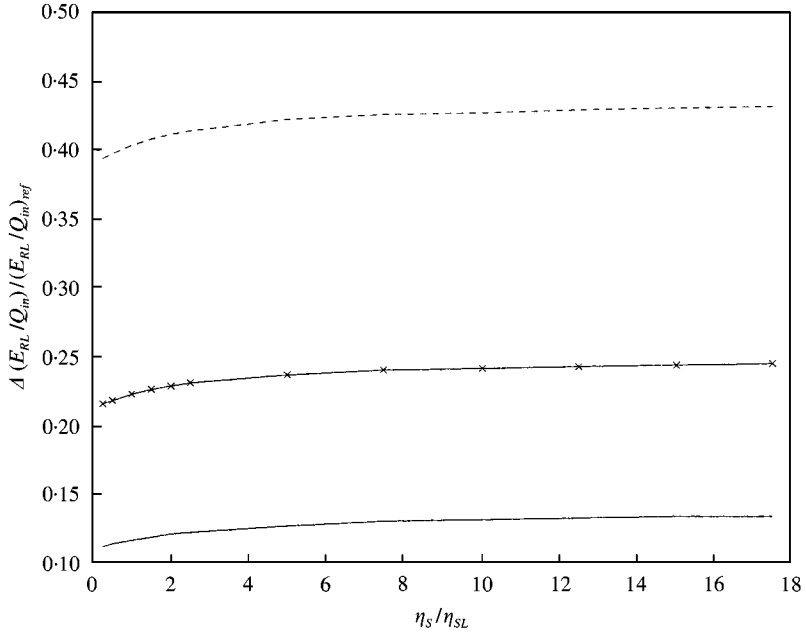

Figure 24. Analytical results for relative variation of E_{RL}/Q_{in} with respect to I_{RL}/I_{SL} versus η_S/η_{SL} in system G: ——, $I_{RL}/I_{SL} = 0{\cdot}5$ and 1·0; —×—, 0·5 and 1·5; – – –, 0·5 and 3·0.

in it for a constant external input power. A higher amount of energy is stored in more flexible receiving members regardless of the amount of damping in the connecting short member. When the damping of the connecting short member increases, a larger amount of energy is dissipated and a smaller amount of power is transferred to the receiving long member. Therefore, for larger values of the relative damping ratio the difference in the amount of energy stored in members with different rigidity decreases.

Results for the relative difference in the energy of the long members for different values of bending rigidity are presented in Figures 23 and 24 for the hybrid FEA and an analytical solution respectively. It can be observed that the relative difference in the energy of the receiving long member is approximately the same for all the values of relative coupling damping. Therefore, the damping of the short member has the same effect on the energy stored in the receiving long member and on its relative difference. Good correlation is observed between the hybrid FEA results (Figures 21 and 23) and the analytical solution (Figures 22 and 24) for all the analyses.

5. CONCLUSIONS

The hybrid FEA is employed in order to investigate several power flow concepts in systems of co-linear beams in the mid-frequency range. Results from analytical solutions are also presented and excellent correlation is observed. It is demonstrated that the hybrid FEA formulation can capture properly the phenomena of power re-injection and power re-radiation. Highly resonant effects that are present in a system in the mid-frequency range are properly accounted in the hybrid FEA. The coupling rigidity and the coupling damping of a short member are important for the power flow through a system. The resonant characteristics of a short member can be utilized in order to increase the isolation between

inter-connected long members. The relative rigidity between a receiving and a source long member has an important effect on the amount of energy stored in the receiving member. The coupling damping affects the amount of energy stored in the receiving member, but has a minimal impact on the relative change in the energy stored in the receiving member. EFEA results are compared, as representative of a high-frequency solution, to hybrid FEA results. It is demonstrated that when the resonant effects of the short member are important, large differences exist between the EFEA and hybrid FEA results.

ACKNOWLEDGMENTS

This research was sponsored by the Automotive Research Center (ARC) established at the Mechanical Engineering and Applied Mechanics Department of the University of Michigan, Ann Arbor, by the U.S. Army/Tank-Automotive and Armaments Command (TACOM).

REFERENCES

1. K. J. BATHE 1982 *Finite Element Procedures in Engineering Analysis*. Englewood Cliffs, NJ: Prentice-Hall.
2. K. H. HUEBNER and E. A. THORNTON 1982 *The Finite Element Method for Engineers*. Wiley, NY, second edition.
3. M. A. GOCKEL (editor) 1983 *MSC/NASTRAN Handbook for Dynamic Analysis*. The MacNeal-Schwendler Corporation.
4. R. H. LYON 1975 *Statistical Energy Analysis of Dynamical Systems*: *Theory and Applications*. Cambridge, MA: The MIT Press.
5. J. WOODHOUSE 1991 *Journal of the Acoustical Society of America* **69**, 1695–1709. An approach to the theoretical background of statistical energy analysis applied to structural vibration.
6. R. S. THOMAS, J. PAN, M. J. MOELLER and T. W. NOLAN 1997 *Noise Control Engineering Journal* **45**, 25–34. Implementing and improving statistical energy analysis models using quality technology
7. C. J. RADCLIFFE and X. L. HUANG 1997 *Journal of Vibration and Acoustics* **119**, 629–634. Putting statistics into the statistical energy analysis of automotive vehicles.
8. C. B. BURROUGHS, R. W. FISCHER and F. R. KERN 1997 *Journal of the Acoustical Society of America* **101**, 1779–1789. An introduction to statistical energy analysis.
9. D. J. NEFSKE and S. H. SUNG 1989 *Journal of Vibration, Acoustics, Stress and Reliability* **111**, 94–106. Power flow finite element analysis of dynamic systems: basic theory and applications to beams.
10. O. M. BOUTHIER and R. J. BERNHARD 1992 *American Institute of Aeronautics and Astronautics Journal* **30**, 138–146. Models of space averaged energetics of plates.
11. O. M. BOUTHIER 1992 *Ph.D. Dissertation, Mechanical Engineering Department, Purdue University, Lafayette, IN*. Energetics of vibrating systems.
12. O. M. BOUTHIER and R. J. BERNHARD 1995 *Journal of Sound and Vibration* **182**, 149–164. Simple models of the energetics of transversely vibrating plates.
13. J. E. HUFF and R. J. BERNHARD 1995 *Proceedings of Inter-Noise* 95, *Newport Beach, CA, July*, 1221–1226. Prediction of high frequency vibrations in coupled plates using energy finite element.
14. N. VLAHOPOULOS, X. ZHAO and T. ALLEN 1999 *Journal of Sound and Vibration* **220**, 135–154. An approach for evaluating power transfer coefficients for spot-welded joints in an energy finite element formulation.
15. R. J. BERNHARD and J. E. HUFF 1999 *Journal of Vibration and Acoustics* **121**, 295–301. Structural–acoustic design at high frequency using the energy finite element method.
16. N. VLAHOPOULOS, L. O. GARZA-RIOS and C. MOLLO 1999 *Journal of Ship Research* **43**, 143–156. Numerical implementation, validation, and marine applications of an energy finite element formulation.
17. L. CREMER, M. HECKL and E. E. UNGAR 1973 *Structure Borne Sound*. New York: Springer-Verlag.

18. N. VLAHOPOULOS and X. ZHAO 1999 *American Institute of Aeronautics and Astronautics Journal* **37**, 1495–1505. Basic development of hybrid finite element method for mid-frequency structural vibrations.
19. B. R. MACE 1992 *Journal of Sound and Vibration* **154**, 321–341. The statistics of power flow between two continuous one-dimensional subsystems.
20. J. S. SUN, C. WANG and Z. H. SUN 1996 *Journal of Sound and Vibration* **189**, 215–229. Power flow between three series coupled oscillators.
21. B. R. MACE 1992 *Journal of Sound and Vibration* **154**, 289–319. Power flow between two continuous one-dimensional subsystems: a wave solution.
22. F. J. FAHY and D. YAO 1987 *Journal of Sound and Vibration* **114**, 1–11. Power flow between non-conservatively coupled oscillators.
23. J. C. SUN, N. LALOR and E. J. RICHARDS 1987 *Journal of Sound and Vibration* **112**, 321–330. Power flow and energy balance of non-conservatively coupled structures, I: theory.
24. N. VLAHOPOULOS, C. VALLANCE and R. D. STARK 1998 *Journal of Spacecraft and Rockets* **35**, 355–360. Numerical approach for computing noise-induced vibration from launch environments.
25. P. CHO 1993 *Ph.D. Dissertation, Mechanical Engineering Department, Purdue University*. Energy flow analysis of coupled structures.
26. B. R. MACE 1992 *Journal of Sound and Vibration* **159**, 305–325. Power flow between two coupled beams.
27. S. FINNVEDEN 1995 *Journal of Sound and Vibration* **187**, 495–529. Ensemble averaged vibration energy flows in a three-element structure.